

Article

Study on the Mechanism of Meseaconitine-Induced Hepatotoxicity in Rats Based on Metabonomics and Toxicology Network

Qian Chen ^{1,†}, Kai Zhang ^{2,†}, Mingjie Jiao ¹, Jiakang Jiao ¹, Dongling Chen ¹, Yihui Yin ¹, Jia Zhang ¹ and Fei Li ^{1,*}

¹ School of Chinese Materia Medica, Beijing University of Chinese Medicine, Liangxiang Town, Fangshan District, Beijing 102488, China; chenqian19980101@foxmail.com (Q.C.); jmj9898@163.com (M.J.); jiaojiaok123@163.com (J.J.); cdl181136@163.com (D.C.); 20190935005@bucm.edu.cn (Y.Y.); zhangjbucm@163.com (J.Z.)

² School of Life Sciences, Beijing University of Chinese Medicine, Liangxiang Town, Fangshan District, Beijing 102488, China; zk006086@163.com

* Correspondence: 602110@bucm.edu.cn; Tel.: +86-132-4543-8896

† These authors contributed equally to this work.

Abstract: Meseaconitine (MA), one of the main diterpenoid alkaloids in *Aconitum*, has a variety of pharmacological effects, such as analgesia, anti-inflammation and relaxation of rat aorta. However, MA is a highly toxic ingredient. At present, studies on its toxicity are mainly focused on the heart and central nervous system, and there are few reports on the hepatotoxic mechanism of MA. Therefore, we evaluated the effects of MA administration on liver. SD rats were randomly divided into a normal saline (NS) group, a low-dose MA group (0.8 mg/kg/day) and a high-dose MA group (1.2 mg/kg/day). After 6 days of administration, the toxicity of MA on the liver was observed. Metabolomic and network toxicology methods were combined to explore the effect of MA on the liver of SD rats and the mechanism of hepatotoxicity in this study. Through metabonomics study, the differential metabolites of MA, such as L-phenylalanine, retinyl ester, L-proline and 5-hydroxyindole acetaldehyde, were obtained, which involved amino acid metabolism, vitamin metabolism, glucose metabolism and lipid metabolism. Based on network toxicological analysis, MA can affect HIF-1 signal pathway, MAPK signal pathway, PI3K-Akt signal pathway and FoxO signal pathway by regulating ALB, AKT1, CASP3, IL2 and other targets. Western blot results showed that protein expression of HMOX1, IL2 and caspase-3 in liver significantly increased after MA administration ($p < 0.05$). Combined with the results of metabonomics and network toxicology, it is suggested that MA may induce hepatotoxicity by activating oxidative stress, initiating inflammatory reaction and inducing apoptosis.

Keywords: meseaconitine; hepatotoxicity; metabonomics; network toxicology; oxidative stress; inflammatory response; apoptosis

Key Contribution: This study suggests that the mechanism of hepatotoxicity induced by Meseaconitine may involve oxidative stress, inflammatory response and apoptosis.



Citation: Chen, Q.; Zhang, K.; Jiao, M.; Jiao, J.; Chen, D.; Yin, Y.; Zhang, J.; Li, F. Study on the Mechanism of Meseaconitine-Induced Hepatotoxicity in Rats Based on Metabonomics and Toxicology Network. *Toxins* **2022**, *14*, 486. <https://doi.org/10.3390/toxins14070486>

Received: 8 June 2022

Accepted: 13 July 2022

Published: 14 July 2022

Publisher's Note: MDPI stays neutral with regard to jurisdictional claims in published maps and institutional affiliations.



Copyright: © 2022 by the authors. Licensee MDPI, Basel, Switzerland. This article is an open access article distributed under the terms and conditions of the Creative Commons Attribution (CC BY) license (<https://creativecommons.org/licenses/by/4.0/>).

1. Introduction

Meseaconitine (MA) is a C₁₉-diterpenoid alkaloid derived from *Aconitum*, which has extensive biological activities and potential toxicity [1]. MA was considered to be one of the most active ingredients of *Aconitum* alkaloids, with analgesic, anti-inflammatory, positive inotropic, antiepileptic, antidepressant and vasodilating effects [2–11]. However, MA is a highly toxic ingredient, and this led to the controversy around using *Aconitum* herbs (such as *Radix Aconiti Lateralis*), which contain MA, in clinical setting. Therefore, it is necessary to systematically study the toxic mechanism of MA to provide reference for the safe clinical use of *Aconitum*.

At present, the toxicity studies on *Radix Aconiti Lateralis* (Fuzi) are mainly focused on its effect on the heart and central nervous system [12–15], and there are few reports on the hepatotoxicity mechanism of Fuzi. However, in recent years, the hepatotoxicity of traditional Chinese medicine has been widely discussed. Studies have shown that liver injury involves oxidative stress, inflammatory response, endoplasmic reticulum stress, apoptosis, cholestasis, immune function and other pathways. Flavonoids of vine tea may promote oxidative stress and pro-oxidative generation of free radicals and attack the mitochondria at the cellular level, causing cytotoxicity, triggering apoptotic mechanisms and causing damage to the liver [16]. Inflammasomes are a group of cellular protein complexes, which are closely related to liver diseases. They can recognize exogenous microorganisms, endogenous danger signals and different stressors, and then activate caspase-1 to produce IL-1 β and IL-18 to initiate inflammation [17]. Studies have shown that acute inflammatory response is related to MAPK activation, NF- κ B signaling induction, NLRP3 inflammasome pathway activation and oxidative stress increase, and the absence of Fpr1 gene expression has a positive effect on inflammation [18]. Direct hepatotoxicity is usually attributable to apoptosis or necrosis. Apoptosis can occur via the extrinsic pathway triggered by the activation of death receptors, such as Fas, and the intrinsic mitochondrial pathway, activated by intracellular perturbations, such as endoplasmic reticulum stress and oxidative damage [19]. It is reported that dose-dependent hepatotoxicity of Fuzi has been clearly observed in preclinical studies [20]. In addition, liver damage has been reported in several toxicity studies of rodents after single or long-term oral administration of Fuzi extract [21,22]. Studies have shown that after oral administration of Fuzi, the level of toxic alkaloids in the liver is very high, which can partly explain the hepatotoxicity of Fuzi, but the mechanism is still unclear [23]. In previous research, our research group screened out 22 potential hepatotoxic ingredients of Fuzi which can induce liver injury in rats [24]. As one of the potential hepatotoxic components of Fuzi, MA needs to be further studied.

At present, the characterization methods of drug toxicity mainly include serum biochemical markers detection and histopathological observation. These methods have certain limitations, and they cannot detect complex and huge metabolites, so it is difficult to evaluate the toxicity of MA in a timely and comprehensive way. Metabonomics is a systematic study of the overall metabolic response to stimulation. The unique metabolic changes induced by drugs reveal tissue damage types and related toxic mechanisms. The concept of analyzing life phenomena from a holistic perspective is very consistent with the treatment ideal of traditional Chinese medicine and is applicable to the study of traditional Chinese medicine [25]. Ultra-high-performance liquid chromatography coupled with quadrupoles hybrid electrostatic field orbital trap high-resolution mass spectrometry (UPLC-Q-Exactive Orbitrap-MS) is cutting-edge detection technology developed in recent years. It combines the advantages of both ultra-high-performance liquid chromatography and high-resolution mass spectrometry, and has characteristics such as high resolution, good quality accuracy and strong qualitative and quantitative capabilities, which make metabonomics analysis more efficient, in depth and accurate. Based on the interaction of “toxicity-gene-target-drug”, network toxicology constructs a complex regulatory network to explore the potential toxic mechanism of the research object, which can explain the molecular basis of disease from a multidimensional perspective. Network toxicology provides the information of enzymes and key proteins in signal pathways, and metabolomics provides the final pathological results. The combination of metabolomics and network toxicology technology can reveal the potential complex relationship between multiple metabolites and multiple targets, mutually verify and supplement from different levels and reveal the mechanism of toxicity [26].

Based on the above research status, this study combined non-targeted metabolomics and network toxicology technology to study the basic toxicity of MA. By analyzing the screened differential metabolites and targets related to hepatotoxicity, as well as the enriched pathway information, we found that the hepatotoxicity of MA may be related to oxidative stress, inflammation and apoptosis. This study not only provides data sup-

port for the toxicity study of MA, but also provides a reference for the toxicity study of Aconitum herbs.

2. Results

2.1. Manifestation of Hepatotoxicity Induced by MA

2.1.1. Analysis of Body Weight and Organ Coefficient

As shown in Figure 1A, after 6 days of administration, compared with the NS group, the weight of rats in the low-dose group of MA tended to decrease, while the weight of the high-dose group decreased significantly ($p < 0.05$). The weight loss may have come from damage to organs caused by MA. The results of the organ coefficient (Figure 1B) showed that, compared with the NS group, the liver coefficient of the low-dose group of MA was decreased, and the liver coefficient of the high-dose group decreased significantly ($p < 0.05$). This suggested that the liver of the MA group may be damaged.

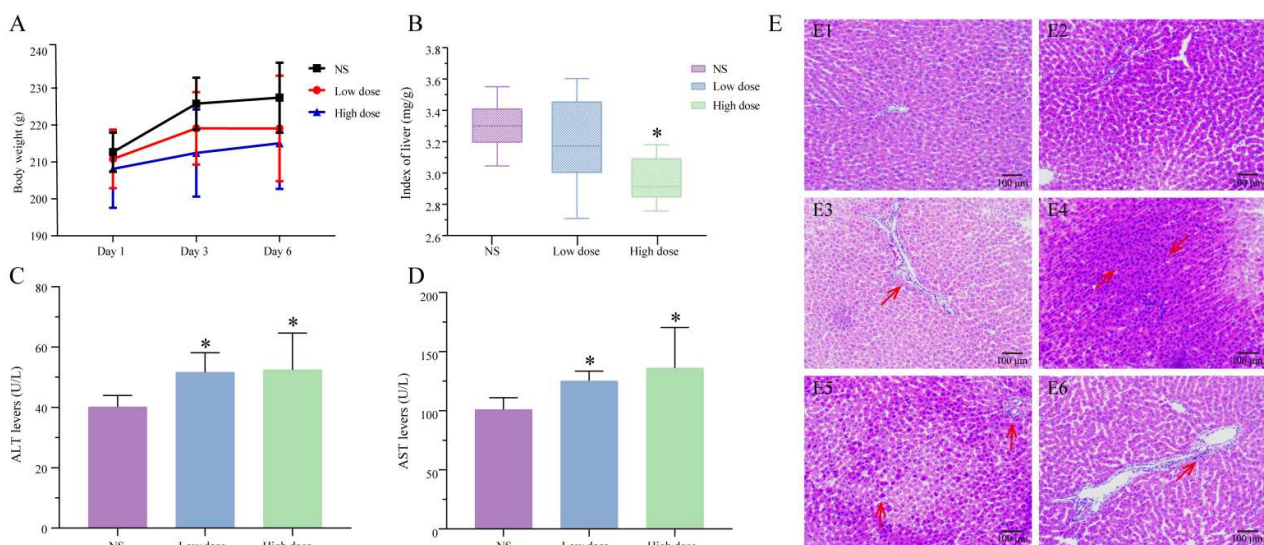


Figure 1. (A) The body weight of rats in the NS group and the MA group increased within 6 days. (B) Index of liver in NS group and MA group (compared with NS group: $* p < 0.05$). Results were analyzed by one-way ANOVA followed by a LSD test for multiple comparisons. (C) Serum ALT levels. The data were analyzed using a Kruskal–Wallis non-parametric test. (D) Serum AST levels. The data were analyzed using a Kruskal–Wallis non-parametric test. (E) Effects of MA on the morphology of liver in rats. NS group (E1,E2), low-dose group (E3,E4), high-dose group (E5,E6), red arrow points to hepatocyte necrosis or inflammatory cell infiltration.

2.1.2. Serum Biochemical Analysis

In this study, the levels of ALT and AST in rat serum were measured to evaluate the degree of liver injury. Results showed that compared with the NS group, the ALT and AST of low-dose and high-dose MA groups were significantly different ($p < 0.05$), and abnormal serum biochemical values indicated that the liver function of the administration group might be damaged (Figure 1).

2.1.3. Analysis of Pathological Results

The histopathological results (Figure 1E) showed that the hepatocytes of the NS group were arranged radially around the central vein, with large and clear nuclei in the center. The structure of liver lobules was complete, and no clear liver injury was found. The sections of low-dose and high-dose groups of MA showed large necrotic areas, including lymphocytes, macrophages and neutrophils, which were large in volume and dark blue in basophilic color. There was inflammatory cell infiltration around the portal area, dense inflammatory cells gathered into pieces and granular degeneration was occasionally seen.

2.2. Metabonomics Study on Hepatotoxicity Induced by MA

2.2.1. Methodology Test

In order to ensure the reliable quality of metabonomics data, the QC samples were tested for methodology. The same QC sample solution was continuously injected six times, and the data were exported as peak areas. RSD values of each ion peak area were calculated, and ions with RSD <30% accounted for 80.02%, indicating that the instrument was stable and had good precision; six QC sample solutions were prepared in parallel, and the samples were continuously injected for analysis. The data were exported as peak areas, and RSD values of each ion peak area were calculated. Ions with RSD <30% accounted for 85.67%, indicating that the method had good repeatability. The same QC sample solution was injected and analyzed at six time points in the whole injection sequence. The data were exported as peak areas, and RSD values of each ion characteristic were calculated. Ions with RSD <30% accounted for 80.08%, indicating that the stability of data collection was very good.

2.2.2. Multivariate Statistical Analysis

The metabolic data were analyzed using PCA and OPLS-DA to explore the effect of MA on metabolism in rats. The data of each group were classified via PCA analysis, and the degree of aggregation and dispersion of samples could be observed. By analyzing the results of PCA (Figure 2A), it can be seen that MA can change endogenous metabolites in rats. The PCA scatterplots of NS group and MA administration group were separated. OPLS-DA is a supervised mode of analysis used to screen for differential metabolites. As shown in Figure 2B, the serum metabolites of NS group and the MA-administered group were completely separated, indicating that MA interfered with the metabolic profile of rats. Two hundred permutation tests were used to evaluate whether the OPLS-DA model was overfitted. The intercept of Q2 at the y -axis was less than zero, indicating that the model had not been overfitted. It was considered that the model was effective and reliable (Figure 2C).

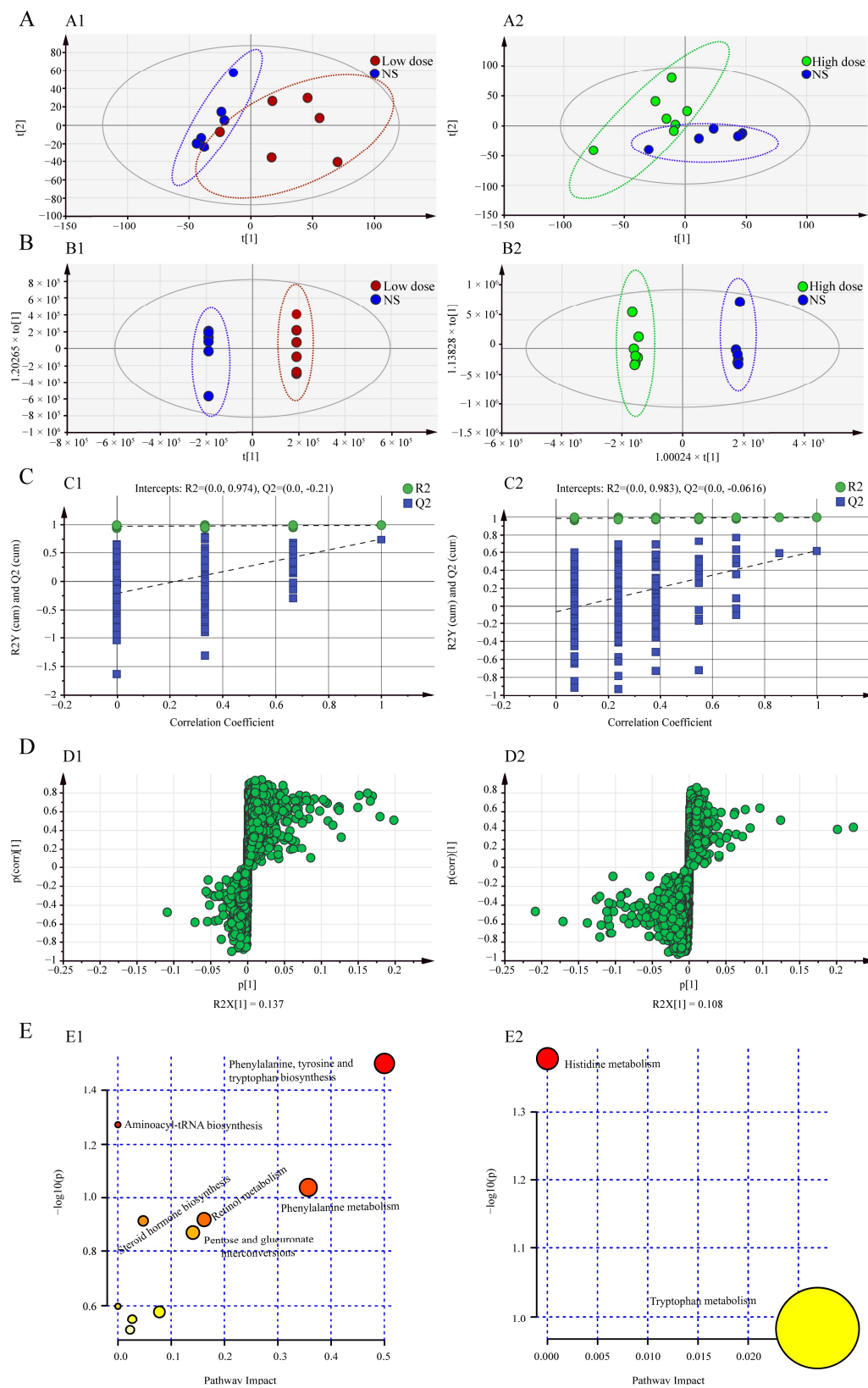


Figure 2. (A) PCA score plot for NS and MA groups. (A1: NS vs. low dose. A2: NS vs. high dose.). (B) OPLS-DA score plot for NS and MA groups. (B1: NS vs. low dose. B2: NS vs. high dose.). (C) Permutation test of OPLS-DA model. (C1: NS vs. low dose. C2: NS vs. high dose.). (D) S-plots obtained from OPLS-DA model. (D1: NS vs. low dose. D2: NS vs. high dose.). (E) Analysis of metabolic pathways. (E1: NS vs. low dose. E2: NS vs. high dose.).

2.2.3. Screening of Differential Metabolites

The differential metabolites after administration of MA were screened by S-plots (Figure 2D) combined with the criteria of $VIP \geq 1$ and $p < 0.05$, and the screened differential metabolites were identified using the HMDB database. A total of 17 differential metabolites were identified in the low-dose group and the NS group, mainly including L-phenylalanine, retinyl ester, aldosterone, L-proline, dehydroepiandrosterone, (4Z,7Z,10Z,13Z,16Z,19Z)-docosahexaenoic acid, β -D-glucuronoside, glycocholic acid, 5-hydroxyindoleacetaldehyde, etc. A total of 13 differential metabolites were identified in the high-dose group and the NS group, mainly including 5-hydroxyindoleacetaldehyde, methylimidazoleacetic acid, etc. (Table 1). By analyzing the differential metabolites between low-dose and high-dose groups of MA, six common differential metabolites were found, namely 5-Hydroxyindoleacetaldehyde, Indole-3-methyl acetate, Indole, MG (0:0/16:0/0:0), 3,5-Tetradecadienecarnitine and Gamma-linolenyl carnitine. Compared with the NS group, these six differential metabolites were upregulated in low-dose and high-dose MA groups, and Indole-3-methyl acetate, 3,5-Tetradecadienecarnitine and Gamma-linolenyl carnitine were upregulated more significantly in the high-dose group, while 5-Hydroxyindoleacetaldehyde, Indole and MG (0:0/16:0/0:0) were upregulated more significantly in the low-dose group. There were 11 unique differential metabolites in the low-dose group of MA, including L-Proline, L-Phenylalanine, Retinyl ester and β -D-Glucuronoside, etc., which were mainly related to amino acid metabolism, glucose metabolism and vitamin metabolism. There were seven unique differential metabolites in the high-dose group of MA, including 2-Hydroxymyristoylcarnitine, Dodecanoylcarnitine and Decanoylcarnitine, etc., which may be related to lipid metabolism.

Table 1. Identification results of potential differential metabolites in rat serum.

| No. | Rt/min | Ion Mode | Obsed m/z | Calcd m/z | Error (ppm) | Formula | Identify | HMDB | Group |
|-----|--------|---------------------|-----------|-----------|-------------|------------|---------------------------------------|-------------|-----------------------|
| 1 | 0.931 | [M+H] ⁺ | 130.08621 | 130.08625 | -0.307 | C6H11NO2 | D-Pipecolic acid | HMDB0005960 | High dose |
| 2 | 1.918 | [M+H] ⁺ | 116.07054 | 116.07060 | -0.517 | C5H9NO2 | L-Proline | HMDB0000162 | Low dose |
| 3 | 2.217 | [M+H] ⁺ | 132.10193 | 132.10190 | 0.227 | C6H13NO2 | D-Leucine | HMDB0013773 | High dose |
| 4 | 2.810 | [M+H] ⁺ | 115.11172 | 115.11174 | -0.174 | C7H14O | 4-Heptanone | HMDB0004814 | High dose |
| 5 | 2.849 | [M+H] ⁺ | 166.08612 | 166.08625 | -0.783 | C9H11NO2 | L-Phenylalanine | HMDB0000159 | Low dose |
| 6 | 3.373 | [M+H] ⁺ | 340.10211 | 340.10269 | -1.705 | C15H17NO8 | 5-Hydroxy-6-methoxyindole glucuronide | HMDB0010363 | Low dose |
| 7 | 3.886 | [M+H] ⁺ | 141.06564 | 141.06585 | -1.489 | C6H8N2O2 | Methylimidazoleacetic acid | HMDB0002820 | High dose |
| 8 | 4.757 | [M+H] ⁺ | 514.28412 | 514.28329 | 1.614 | C26H43NO7S | Sulfolithocholylglycine | HMDB0002639 | Low dose |
| 9 | 4.901 | [M+H] ⁺ | 176.07085 | 176.07060 | 1.420 | C10H9NO2 | 5-Hydroxyindoleacetaldehyde | HMDB0004073 | Low dose High dose |
| 10 | 5.909 | [M+H] ⁺ | 190.08615 | 190.08625 | -0.526 | C11H11NO2 | Indole-3-methyl acetate | HMDB0029738 | Low dose High dose |
| 11 | 6.336 | [M+H] ⁺ | 361.19955 | 361.20095 | -3.876 | C21H28O5 | Aldosterone | HMDB0000037 | Low dose |
| 12 | 7.945 | [M+H] ⁺ | 466.31470 | 466.31631 | -3.453 | C26H43NO6 | Glycocholic acid | HMDB0000138 | Low dose |
| 13 | 8.033 | [M+H] ⁺ | 289.21573 | 289.21620 | -1.625 | C19H28O2 | Dehydroepiandrosterone | HMDB0000077 | Low dose |
| 14 | 8.034 | [M+H] ⁺ | 118.06486 | 118.06512 | -2.202 | C8H7N | Indole | HMDB0000738 | Low dose High dose |
| 15 | 8.536 | [M+Na] ⁺ | 351.23093 | 351.22945 | 4.214 | C22H32O2 | Docosahexaenoic acid | HMDB0002183 | Low dose |
| 16 | 8.823 | [M+K] ⁺ | 369.24194 | 369.24016 | 4.821 | C19H38O4 | MG (0:0/16:0/0:0) | HMDB0011533 | Low dose High dose |
| 17 | 9.351 | [M+H] ⁺ | 314.23276 | 314.23258 | 0.573 | C17H31NO4 | 9-Decenoylcarnitine | HMDB0013205 | Low dose |
| 18 | 10.480 | [M+H] ⁺ | 316.24741 | 316.24823 | -2.593 | C17H33NO4 | Decanoylcarnitine | HMDB0000651 | High dose |
| 19 | 12.718 | [M+H] ⁺ | 368.27847 | 368.27953 | -2.878 | C21H37NO4 | 3,5-Tetradecadienecarnitine | HMDB0013331 | Low dose High dose |
| 20 | 12.733 | [M+H] ⁺ | 388.30527 | 388.30574 | -1.210 | C21H41NO5 | 2-Hydroxymyristoylcarnitine | HMDB0013166 | High dose |
| 21 | 12.750 | [M+H] ⁺ | 295.22559 | 295.22677 | -3.997 | C18H30O3 | 9-OxoODE | HMDB0004669 | Low dose |
| 22 | 13.111 | [M+H] ⁺ | 344.28049 | 344.27953 | 2.788 | C19H37NO4 | Dodecanoylcarnitine | HMDB0002250 | High dose |
| 23 | 14.109 | [M+H] ⁺ | 303.23233 | 303.23185 | 1.583 | C20H30O2 | Retinyl ester | HMDB0003598 | Low dose |
| 24 | 18.521 | [M+H] ⁺ | 422.32602 | 422.32648 | -1.089 | C25H43NO4 | Gamma-linolenyl carnitine | HMDB0006318 | Low dose High dose |

2.2.4. Metabolic Pathway Analysis

The screened differential metabolites were imported into Metabo Analyst 5.0 for metabolic pathway analysis, and the results are shown in Table 2. Trends of differential metabolites involved in metabolic pathways are shown in Table S1. As shown in Figure 2E, there were 10 metabolic pathways involved in differential metabolites between the low-dose group of MA and the NS group, mainly including phenylalanine, tyrosine and tryptophan biosynthesis, phenylalanine metabolism, retinol metabolism, arginine and proline metabolism, tryptophan metabolism and aminoacyl-tRNA biosynthesis, etc. The differential metabolites of the high-dose group and the NS group involved two metabolic pathways, namely tryptophan metabolism and histidine metabolism. By analyzing the metabolic pathways of low-dose and high-dose groups of MA, it was found that tryptophan metabolism was involved in both low-dose and high-dose groups. In addition, the low-dose group involved nine unique metabolic pathways, including phenylalanine metabolism, retinol metabolism, arginine and proline metabolism, etc. Histidine metabolism was a unique pathway in the high-dose group. The summarized metabolic pathways in the low-dose and high-dose rats are shown in Figure S1. It can be seen that MA can affect amino acid metabolism, vitamin metabolism, glucose metabolism and lipid metabolism.

Table 2. Analysis results of metabolic pathways related to differential metabolites.

| No. | Metabolic Pathway | Metabolite | p | −Log(p) | Holm p | FDR | Impact | Group |
|-----|---|--|--------------------|-------------------|--------|-----|---------|-----------------------|
| 1 | Phenylalanine, tyrosine and tryptophan biosynthesis | L-Phenylalanine | 0.031463 | 1.5022 | 1.0 | 1.0 | 0.5 | Low dose |
| 2 | Histidine metabolism | Methylimidazoleacetic acid | 0.041783 | 1.379 | 1.0 | 1.0 | 0.0 | High dose |
| 3 | Aminoacyl-tRNA biosynthesis | L-Phenylalanine; L-Proline | 0.05338 | 1.2726 | 1.0 | 1.0 | 0.0 | Low dose |
| 4 | Phenylalanine metabolism | L-Phenylalanine | 0.091683 | 1.0377 | 1.0 | 1.0 | 0.35714 | Low dose |
| 5 | Retinol metabolism | Retinyl ester | 0.12049 | 0.91906 | 1.0 | 1.0 | 0.16168 | Low dose |
| 6 | Steroid hormone biosynthesis | Dehydroepiandrosterone; Aldosterone | 0.12185 | 0.91416 | 1.0 | 1.0 | 0.0474 | Low dose |
| 7 | Pentose and glucuronate interconversions | beta-D-Glucuronoside | 0.13457 | 0.87104 | 1.0 | 1.0 | 0.14062 | Low dose |
| 8 | Biosynthesis of unsaturated fatty acids | (4Z,7Z,10Z,13Z,16Z,19Z)-Docosahexaenoic acid | 0.25235 | 0.59799 | 1.0 | 1.0 | 0.0 | Low dose |
| 9 | Arginine and proline metabolism | L-Proline | 0.26449 | 0.57759 | 1.0 | 1.0 | 0.0778 | Low dose |
| 10 | Tryptophan metabolism | 5-Hydroxyindoleacetaldehyde | 0.28236 0.10443 | 0.5492 0.98117 | 1.0 | 1.0 | 0.02691 | Low dose High dose |
| 11 | Primary bile acid biosynthesis | Glycocholic acid | 0.31125 | 0.50689 | 1.0 | 1.0 | 0.02285 | Low dose |

2.3. Network Toxicological Study on Hepatotoxicity Induced by MA

2.3.1. Acquisition of “MA-Targets”

A total of 299 targets were obtained from Pharm Mapper database, and 136 targets with Fit >3 were screened. The Swiss TargetPrediction database obtained 17 targets. After integrating and deduplicating the targets of two databases, 152 new aconitine targets were obtained.

2.3.2. Acquisition of “Hepatotoxicity-Targets”

A total of 36 keywords related to hepatotoxicity were searched. By searching the keywords one by one, 10,250 genes with “marker/mechanism” were found in the CTD database, and 93,874 genes with “score > 40” were found in the GeneCards database. The details are shown in Table S2. A total of 552 targets were obtained after integration and deduplication of two online databases. At the same time, the chips were analyzed using R language: GSE103842, GSE113618, GSE116149, GSE119019, GSE129507 and GSE135079. In total, 84 differentially expressed genes were obtained. All the results were integrated and deduplicated, and finally, 634 hepatotoxic targets were obtained.

2.3.3. Construction of Common Target Based on Pathoy Language

The common targets of MA-induced hepatotoxicity in rats were introduced into pathoy, and 31 common targets were obtained. The results are shown in Figure 3A, and the information of these common targets is shown in Table S3.

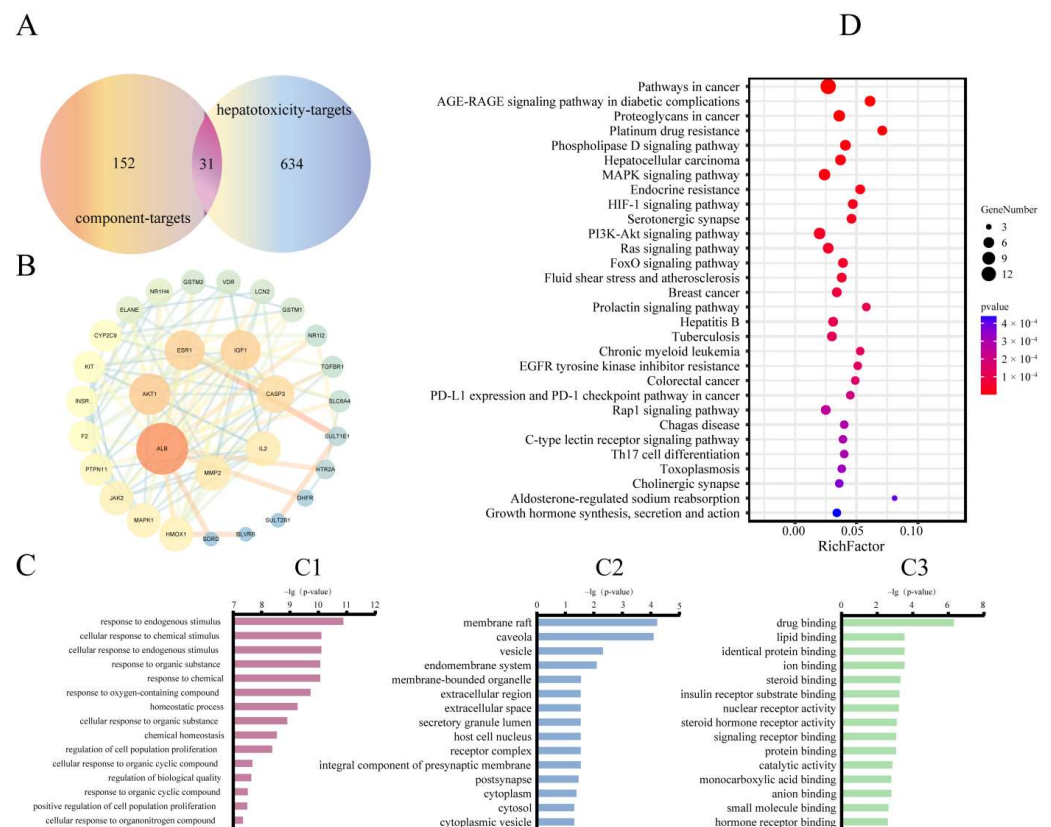


Figure 3. Analysis results of network toxicology. (A) Venn diagram of 31 potential “common targets” was intersected by “component targets” and “hepatotoxicity targets”. (B) Protein–protein interaction (PPI) network. (C) Top 15 items of Go analysis. (C1: biological process. C2: cellular component. C3: molecular function.) (D) Enrichment analysis of KEGG pathways.

2.3.4. Construction and Analysis of PPI Network

The 31 common targets were imported into String for analysis, and the obtained results were imported into Cytoscape 3.7.2 for visualization. The results are shown in Figure 3B. The PPI network graph contains 30 nodes and 116 edges. The size and color of nodes are related to the “Degree” value. The targets with “Degree > 10” include ALB, AKT1, ESR1, IGF1, CASP3, IL2 and MMP2, and their nodes are larger and redder.

2.3.5. Enrichment Analysis of GO and KEGG Pathways

The GO analysis results are shown in Figure 3C. The biological process enriched 491 items, mainly including “response to endogenous stimulus”, “cellular response to chemical stimulus”, “response to organic substance” and “response to oxygen-containing compound”. There were 15 cellular components, mainly including “membrane raft”, “caveola” and “vesicle”. There were 44 molecular functions, including “drug binding”, “lipid binding”, “identical protein binding”, “ion binding” and others. The KEGG pathway analysis results are shown in Figure 3D. A total of 122 pathways were enriched, and the top 30 pathways were selected for visual analysis according to the P value from small to large.

2.4. Effect of MA on Protein Expression of HMOX1, IL2 and Caspase-3 in Liver Tissue

As shown in Figure 4, compared with the NS group, the protein expression of HMOX1, IL2 and caspase-3 in the low-dose group and the high-dose group significantly increased after MA administration ($p < 0.05$).

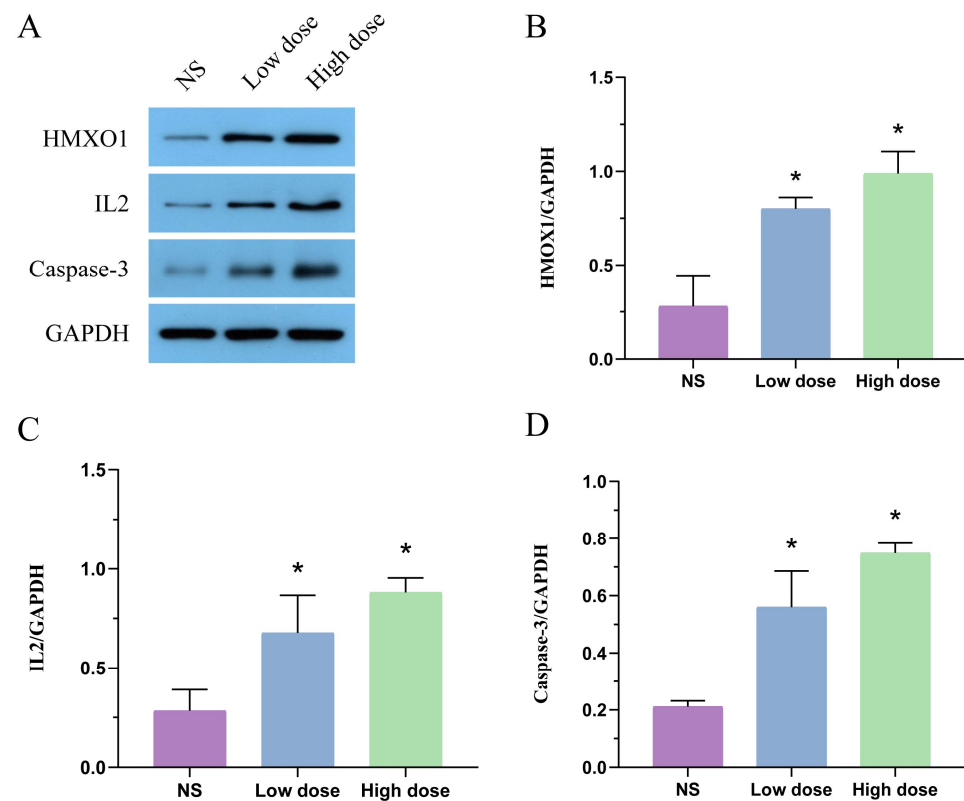


Figure 4. The protein expressions of HMOX1 (A,B), IL2 (A,C), caspase-3 (A,D) in liver tissue were detected by Western blot. Compared with the NS group, * $p < 0.05$.

3. Discussion

3.1. Manifestation of Hepatotoxicity Induced by MA

MA is a diester alkaloid derived from Aconitum, which possesses analgesic, anti-inflammatory and antiepileptic effects. At the same time, MA is also a highly toxic ingredient. The Median lethal dose (LD₅₀) of MA in mice is 1.9 mg/kg, and the half-life is about

2.8–5.8 h [27]. In this study, after continuous administration of MA to rats for 6 days, the body weight and liver coefficient of the low-dose group were lower than those of the NS group, and the body weight and liver coefficient of the high-dose group were significantly different from the NS group ($p < 0.05$), suggesting that MA may cause liver damage in rats. ALT and AST are two membrane-bound enzymes related to liver dysfunction. The increase in ALT and AST levels in serum of rats treated with MA may be due to the increase in membrane permeability caused by oxidative stress, and ALT and AST are released from liver to serum [28]. In addition, according to the pathological sections of liver tissue, the treatment with MA resulted in typical hepatotoxic characteristics, such as hepatocyte necrosis and apoptosis, and infiltration of inflammatory cells around the portal area, indicating that MA has toxic effects on liver, which should be used with caution in clinical practice.

3.2. The Mechanism of Hepatotoxicity Induced by MA

According to the results of metabonomics and network toxicology, we found that MA may induce hepatotoxicity by activating oxidative stress, initiating inflammatory response and inducing apoptosis.

Oxidative stress is an unbalanced state in which reactive oxygen species (ROS) formation in vivo exceeds the antioxidant capacity of cells, resulting in the production of a large number of oxidative intermediates, inflammatory infiltration of neutrophils, increased secretion of protease and others. Our results showed that MA could affect the HIF-1 signaling pathway, increase protein expression of heme oxygenase 1 (HMOX1), downregulate the proline level and disorder tryptophan metabolism, resulting in oxidative stress damage. The HIF-1 signaling pathway enriched by network toxicology is one of the most important pathways involved in the regulation of oxygen homeostasis [28–30]. Hypoxia-inducible factor-1 (HIF-1) is a nuclear protein produced by cells under hypoxic conditions, in which HIF-1 α subunit, as a key factor to respond to hypoxic stress, is regulated by hypoxic signals. HIF-1 can reduce mitochondrial stress by inhibiting mitochondrial division, improving mitochondrial oxygen metabolism, neutralizing ROS and regulating inflammatory response [31]. Studies have shown that stimulation of HIF-1 increases mitochondrial damage and accelerates liver injury [32]. Ubiquitination of HIF-1 α is oxidation of its proline-by-proline hydroxylase, which is then recognized by ubiquitinase von Hippel-Lindau (VHL) for degradation. Blocked ubiquitination of HIF-1 α can cause a series of oxygen homeostasis regulation responses in tissue cells. Proline is known as the elite of non-enzymatic antioxidants. Proline and hydroxyproline (metabolites of proline) have antioxidant properties that can scavenge reactive oxygen species, stabilize and upregulate antioxidant enzyme activity [33], improve cellular resistance to hydrogen peroxide and balance intracellular redox homeostasis, so proline is known as the elite of non-enzymatic antioxidants. Exogenous supplementation of L-proline can enhance the antioxidant capacity of rats [34]. The results of metabonomics showed that proline metabolism was disordered, and excessive production of ROS caused by downregulation of proline would lead to intracellular damage of biomolecules, including cell cycle blocking, autophagy and apoptosis [35]. HMOX1 is a downstream target gene of HIF-1 α . HMOX1 is the most easily induced antioxidant enzyme in organisms discovered so far, and HMOX1 compensatory increases under oxidative stress [36]. The expression of HMOX1 in liver was significantly increased, suggesting that MA may cause oxidative stress injury and induce stress, increasing antioxidant protein HMOX1. 5-hydroxyindoleacetaldehyde is an intermediate metabolite of tryptophan metabolism, which can be biosynthesized from serotonin through the interaction with the enzyme kynurenine 3-monooxygenase. 5-hydroxyindoleacetaldehyde participates in many enzymatic reactions in the human body. Its upregulation caused by MA will inevitably affect the stability of tryptophan metabolism, cause oxidative stress and affect normal physiological functions [37,38].

Inflammation is a kind of defensive response of the body to stimulation, and current studies have clearly shown that hepatotoxic injury involves inflammatory response. Rhein exerts pro-inflammatory actions by increasing the interleukin-1 beta (IL-1 β) and high-

mobility group box-1(HMGB1) release, while downstream pro-inflammatory cytokines will, in turn, promote upstream intracellular signaling cascades and result in positive feedback pro-inflammatory signaling pathways. This amplifying mechanism of inflammatory signal pathways will eventually lead to further liver injury [39]. In this study, MA regulates inflammatory response through IL-2 and downstream PI3K-Akt signaling pathway and MAPK signaling pathway. Downregulation of phenylalanine metabolism and retinol metabolism disorder also proves that MA induces hepatotoxicity by initiating an inflammatory response. Interleukin-2 (IL-2), the target of network toxicology, is a cytokine that regulates innate and adaptive systems [40]. As a T-cell growth factor, IL-2 can promote proliferation of T cells and NK cells and promote B cells to produce antibodies and participate in immune response. Studies have shown that IL-2 can induce hepatic Kupffer cells, monocytes and macrophages to secrete TNF- α [41,42]. TNF- α causes direct cellular damage to liver by inducing production of chemokines, reactive oxygen species and adhesion molecules [43], and is a main inflammatory mediator of liver injury [44]. Western blot results show that IL-2, a cytokine related to inflammation, was upregulated in liver after MA administration, which mediates the inflammatory response. There are three main downstream signal pathways of IL-2, namely PI3K-AKT signal pathway, MAPK signal pathway and JAK-STAT signal pathway. PI3K can regulate NF- κ B and its downstream proinflammatory cytokines [45–47]. Blocking PI3K/Akt will lead to an increase in NF- κ B transcription and release of TNF- α , IL-1 β and IL-6 [48]. Shen's studies have shown that activation of PI3K/Akt signaling pathway increases expression of IL-4 and IL-10, decreases expression of IL-1 β and TNF- α and reduces hepatic inflammatory response [49]. Studies have found that deletion of Akt1 and Akt2 in the liver can induce liver inflammation and hepatocyte death, and the use of PI3K/Akt inhibitors can significantly increase the degree of liver damage in mice [50]. In addition, the MAPK signaling pathway is also involved in inflammatory response [51]. Hydroxytyrosol (HT) administration is able to reduce colon inflammation, swelling, inflammatory cell infiltration and cytokine and chemokine overexpression [52], and HT increases the level of anti-inflammatory cytokines through the MAPK pathway [53]. Studies have shown that MAPK signaling cascade plays a key role in drug-induced hepatotoxicity by interacting with various signaling pathways [54–58]. Phenylalanine is an essential aromatic amino acid for the human body, which is very important for maintaining various functions and normal growth of the body. Phenylalanine is metabolized into tyrosine by the liver. However, when the liver is damaged, phenylalanine hydroxylase (PAH) will be destroyed, and the conversion of phenylalanine to tyrosine will be blocked, resulting in excessive phenylalanine concentration in the blood. Studies have shown that concentration of phenylalanine in plasma is positively correlated with the level of alanine aminotransferase (reflecting the degree of liver injury), and phenylalanine is a good biomarker for the severity of acute liver failure. Metabonomics results showed that phenylalanine was upregulated, indicating that liver function was impaired. Inflammation plays a key role in the increase in phenylalanine levels [59]. Inflammation-induced ROS production may consume a large part of tetrahydrobiopterin (BH4) [60]. BH4 is a cofactor of PAH, which directly affects activity of PAH, resulting in downregulation of the phenylalanine metabolism. The retinol metabolic pathway enriched by metabonomics is also closely related to liver. When liver is stimulated, retinoic acid can promote expression of RAE-1 (ligand of NKG2D receptor) in activated hepatic stellate cells and inhibit TGF- β /Smad3 signal, thereby improving the killing ability of NK cells and regulating inflammatory response.

Apoptosis is a spontaneous and orderly death, and its process is extremely complex. It is closely related to production of oxygen free radicals, disorder of cell energy metabolism, activation of cytokines, intracellular calcium overload and expression of cysteine protease (caspase) and B lymphocyte tumor-2 (Bcl-2) family genes. The disorder of apoptosis mechanism can induce a variety of diseases [61]. There are three main pathways of apoptosis, including mitochondrial apoptosis pathway, endoplasmic reticulum pathway and death receptor pathway. Mitochondrial pathway and endoplasmic reticulum stress belong to the

endogenous pathway, and death receptor pathway belongs to the exogenous pathway. The endogenous pathway is mainly regulated by Bcl-2 family proteins, while the exogenous pathway is mainly regulated by caspase [62]. Caspase is a key mediator of programmed cell death or apoptosis, and it plays an important role in mediating apoptosis [63,64]. In this study, CASP3, the target of network toxicology, is the most important downstream effector molecule of orderly apoptosis cascade, and its activation is a sign of irreversible apoptosis [29]. Western blot results show that protein expression of caspase-3 in liver increased significantly after administration of MA, suggesting increased apoptosis. Activated caspase-3 can promote the cleavage of caspase-8 and amplify the pro-apoptotic signal pathway through mitochondria [65]. In addition, a large amount of evidence shows that the FoxO signaling pathway is also closely related to apoptosis, such as B cells, T cells, macrophages, neurons and glioma cells [66–69]. FoxO transcription factors belong to the Forkhead protein family, and their members include FoxO1, FoxO3, FoxO4 and FoxO6. One of the main expression sites of FoxO1 is hepatocytes, and its transcriptional regulation and signal transduction pathways are crucial for important physiological and pathological processes such as hepatocyte proliferation, apoptosis and cell cycle [70]. Studies have shown that reducing expression of p-FoxO1 can induce FoxO1 to enter the nucleus, thus activating the downstream apoptosis signal pathway [71]. The shuttle of FoxO between cytoplasm and nucleus is a key step in apoptosis [72]. In this study, CASP3 and FoxO signal pathway were obtained through network toxicology, and the target CASP3 was verified by Western blotting, which indicated that MA might induce hepatocyte apoptosis through them, thus leading to hepatotoxicity.

3.3. Limitations of the Study

This study combined metabolomics and network toxicology to comprehensively analyze the mechanism of MA-induced hepatotoxicity, but further research is still necessary. Firstly, there are some differences in the disturbance of endogenous metabolites between the high- and low-dose groups of MA, and the mechanism is not clear; secondly, the identification of endogenous differential metabolites in metabolomics completely depends on the online databases, which may lead to false positive results; finally, network toxicology is based on computer virtual computing and network database retrieval, and in vivo and in vitro experiments are necessary ways to further explore its mechanism. In this study, the targets of HMOX1, IL2 and CASP3 were verified by Western blotting. The systematic study of gene expression by transcriptomics and other techniques could further improve the mechanism of MA-induced hepatotoxicity. Based on the above points, future research will focus on a certain pathway for cell and animal experiments to further explore the hepatotoxicity mechanism of MA.

4. Conclusions

In conclusion, this study combined metabolomics and network toxicology to explore the hepatotoxicity mechanism of MA. Through metabolomics study, the differential metabolites of MA, such as L-phenylalanine, retinyl ester, L-proline and 5-Hydroxyindoleacetaldehyde, were obtained, which involved amino acid metabolism, vitamin metabolism, glucose metabolism and lipid metabolism. Based on the network toxicology analysis of online databases and multiple computer languages, 31 key targets of hepatotoxicity induced by MA, such as ALB, AKT1, CASP3 and IL2, were obtained. Western blot results show that protein expression of HMOX1, IL2 and caspase-3 in liver increased significantly ($p < 0.05$) after administration of MA. These targets were enriched by KEGG to obtain key cellular signal transduction pathways, such as HIF-1 signal pathway, MAPK signal pathway, PI3K-Akt signal pathway and FoxO signal pathway. The results of metabolomics and network toxicology further analyzed that MA might induce hepatotoxicity by activating oxidative stress, initiating inflammatory reaction and inducing apoptosis. The results provide data support for the toxicity study of MA and provide a reference for the toxicity study of Aconitum herb.

5. Materials and Methods

5.1. Materials and Animals

5.1.1. Instruments

UPLC-Q-Exactive Orbitrap-MS (Thermo Fisher Scientific, Waltham, MA, USA); automatic biochemical analyzer (Beckman Coulter, Indianapolis, IN, USA); electronic balance (Sartorius, Gottingen, Germany); high-speed centrifuge (Thermo Fisher Scientific); vortex mixer (Dragon Laboratory Instruments Limited, Beijing, China); electrophoresis apparatus (Beijing Kaiyuan Xinrui Instrument Co., Ltd., Beijing, China).

5.1.2. Reference Standards and Reagents

Mesaconitine (Batch number 110799-201608, China Institute for food and drug control); 4% paraformaldehyde tissue fixative (Beijing solabao Technology Co., Ltd., Beijing, China); sodium chloride injection (Shijiazhuang siyao Co., Ltd., Shijiazhuang, China); mass spectrometric formic acid (Thermo Fisher Scientific); mass spectrometric acetonitrile (Thermo Fisher Scientific); protease inhibitor cocktail (ROCHE); protein marker (Thermo). SDS-PAGE gel preparation kit, Ripa total protein lysate, BCA protein concentration determination kit, ECL chemiluminescence detection kit, TBS (powder), electrophoresis solution (powder), membrane transfer solution (powder), antibody eluent, Tween-20 and skimmed milk powder were all purchased from Wuhan baiqiandu Biotechnology Co., Ltd., Wuhan, China.

5.1.3. Experimental Animals and Groups

Thirty-seven clean male SD rats weighing 180–200 g were purchased from SBF Biotechnology Co., Ltd. (Beijing, China) with the license number “SCXK (Jing) 2019-0010”. The rats were raised in the animal laboratory of Liangxiang campus of Beijing University of Chinese Medicine. They were raised under the following controlled environmental conditions: temperature 23 ± 2 °C, humidity $35 \pm 5\%$, and 12 h day–night shift. Adaptive feeding was carried out for 7 days before the experiment, drinking water was provided for an unlimited time and feeding food was provided freely. Rats were randomly divided into three groups: high-dose group ($n = 16$, 1.2 mg/kg/day), low-dose group ($n = 11$, 0.8 mg/kg/day) and normal saline (NS) group ($n = 10$, 8.0 mL/kg/day). The administration scheme for rats is shown in Table 3.

Table 3. Administration scheme of MA.

| Grouping | Number | Drug | Dose | Method of Administration | Exposure Period |
|-----------|--------|-----------|---------------|---------------------------------|-----------------|
| NS | 10 | 0.9% NaCl | 8.0 mL/kg/day | p.o., Continuous administration | 6 days |
| Low dose | 11 | MA | 0.8 mg/kg/day | p.o., Continuous administration | 6 days |
| High dose | 16 | MA | 1.2 mg/kg/day | p.o., Continuous administration | 6 days |

All experimental procedures were conducted in accordance with China’s national legislation and local guidelines. The animal experiment was approved by the Animal Ethics Committee of Beijing University of Chinese Medicine (BUCM-4-2021071901-3023).

5.2. Manifestation of Hepatotoxicity Induced by MA

5.2.1. Body Weight and Organ Coefficient

The rats were weighed and recorded before daily administration. After 6 days of administration, livers of all rats were weighed, and liver coefficients were calculated. The liver coefficient was calculated by dividing the weight of individual rat by the weight of the liver of that rat. The increase in the liver coefficient indicates that liver may have

edema, hyperemia or hypertrophy; conversely, it indicates liver atrophy or other degenerative changes.

5.2.2. Detection of Serum Biochemical Indexes

Rats were administrated continuously for 6 days. After fasting for 12 h, rats were anesthetized with 10% chloral hydrate at a dose of 3 mL/kg. Subsequently, 5 mL blood samples were collected from the abdominal aorta of rats. The whole blood was placed in a test tube and centrifuged at 3000 r/min and 4 °C for 15 min. The supernatant was centrifuged at 3500 r/min and 4 °C for 8 min. The serum obtained was used for serum biochemical detection and metabonomics research. Next, 150 µL was extracted from each serum sample, measured in an automatic biochemical analyzer, and the data of alanine aminotransferase (ALT) and aspartate aminotransferase (AST) were recorded.

5.2.3. Histopathological Examination

The rat liver was removed and washed with normal saline to remove bloodstains. Filter paper was used to remove the surface water to dry the liver sample, which was then fixed in 4% polyformaldehyde solution. Paraffin sections of liver were prepared, and liver sections were stained with hematoxylin–eosin. The pathological manifestations were observed under a microscope for histological examination and evaluation.

5.3. Metabonomics Study on Hepatotoxicity Induced by MA

5.3.1. Sample Preparation

Serum Sample Preparation

The serum samples stored in the –80 °C refrigerator were taken out and thawed at room temperature. Then, 450 µL of acetonitrile was added to 150 µL of serum, sonicated in an ice-water bath for 10 min, vortexed for 1 min, centrifuged at 13,000 rpm for 15 min at 4 °C and the supernatant was taken. The supernatant was blown dry with nitrogen, then 75 µL of 70% acetonitrile was added to redissolve, and followed by centrifugation at 13,000 rpm for 15 min at 4 °C. Finally, the supernatant was placed in a liquid phase vial with a lined tube.

QC Sample Preparation

All samples from the NS group and the administration group were drawn and mixed in equal amounts, and QC samples were prepared according to the method described in the Serum Sample Preparation part.

5.3.2. Analysis Conditions

Chromatographic Conditions

C18 chromatographic column (Waters ACQUITY UPLC HSS T3 Column, polar endcapping, 2.1 mm × 100 mm, 1.8 µm); column temperature—30 °C; sample tray temperature—4 °C. Mobile phase A is 0.1% formic acid water and mobile phase B is acetonitrile. Elution conditions—0~3 min, 4~30% B; 3~7 min, 30~37% B; 7~10 min, 37~60% B; 10~21 min, 60~100%B; 21~21.5 min, 100% B; 21.5~22.5 min, 100~4% B; 22.5~26 min, 4% B. Flow rate—0.3 mL/min; sample volume—3 µL.

Mass Spectrometric Conditions

HESI ion source; positive ionization mode; ionization temperature—350 °C; scanning range— m/z 100–1500; primary scanning resolution—35,000; ionization source voltage—4 kV; capillary voltage—35 V; tube lens voltage—110 V; normalized collision energy—20%, 30%, 40%; sheath gas flow rate—40 arb; auxiliary gas flow rate—20 arb; both are nitrogen.

5.3.3. Methodology Test

Instrument Precision

The same QC sample solution was continuously injected 6 times, and the data were exported as peak areas. RSD values of each ion peak area were calculated, and ions with RSD < 30% should account for more than 80%.

Method Reproducibility

Six QC sample solutions were prepared in parallel, and the samples were continuously injected for analysis. The data were exported as peak areas, and RSD values of each ion peak area were calculated. Ions with RSD < 30% should account for more than 80%.

Sample Stability

The same QC sample solution was injected and analyzed at 6 time points in the whole injection sequence. The data were exported as peak areas, and RSD values of each ion characteristic were calculated. Ions with RSD < 30% should account for more than 80%.

5.3.4. Data Processing

MS-DIAL 4.70 software was used to perform non-linear correction in time domain and automatic integration and extraction of peak intensity for LC-MS data. Xcalibur 4.2 workstation was used to analyze and sort the data and control quality deviation range $\delta \leq 5 \times 10^{-6}$. According to the information of excimer ion peaks and ion fragments obtained by mass spectrometry, combined with literature search and relying on the HMDB database, metabolites were compared. Serum samples of each group were analyzed via principal component analysis (PCA) and partial least squares analysis (OPLS-DA) using SIMCA 14.1 software. Screening conditions: $VIP \geq 1$ and $p \leq 0.05$ as differential metabolites. MetaboAnalyst 5.0 was then used to enrich metabolic pathways.

5.4. Network Toxicological Study on Hepatotoxicity Induced by MA

5.4.1. Acquisition of “MA-Targets”

Firstly, the two-dimensional structural formula of MA was obtained by PubChem (<https://pubchem.ncbi.nlm.nih.gov/>, accessed on 5 April 2022) and uploaded to PharmMapper (<http://www.lilab-ecust.cn/pharmmapper/submitfile.html>, accessed on 5 April 2022), which was used to obtain potential targets of MA. Then, the non-standard gene names obtained by Pharm Mapper were imported into Uniprot (<http://www.uniprot.org/>, accessed on 13 April 2022) to be converted into standard gene names, and the condition was defined as human in the popular organisms item. At the same time, we logged into Swiss TargetPrediction (<http://www.swisstargetprediction.ch/>, accessed on 13 April 2022), uploaded the two-dimensional structural formula of MA and obtained potential targets. Finally, the genes obtained from the two databases were integrated and de-duplicated, and MA-targets were obtained.

5.4.2. Acquisition of “Hepatotoxicity-Targets”

We searched the keyword “liver injury” in PubMed (<https://www.ncbi.nlm.nih.gov/>, accessed on 1 March 2020) to obtain the most comprehensive keywords related to hepatotoxicity. Then, we logged on to CTD (<http://ctdbase.org/>, accessed on 1 March 2020) and Genecards (<http://www.genecards.org/>, accessed on 1 March 2020) to search the keywords related to hepatotoxicity one by one. The genes with “marker/mechanism” were screened using the CTD database, and the genes with “score > 40” were screened using the Genecards database.

In addition, the targets related to hepatotoxicity were mined through the GEO database. The gene expression profile chip data were imported into R language, data were cleaned and formatted and probe names were translated. Then, the differential expression genes were obtained using the linear regression model limma package. The setting conditions of “topTable” function: $p < 0.05$, $\logFC > 2$.

Finally, all the obtained genes were integrated and de-duplicated to obtain “hepatotoxicity-targets”.

5.4.3. Construction of Common Target Based on Pathway Language

The data of MA-targets and hepatotoxicity-targets were imported into pathway, and the “venn2” function under the “matplotlib_venn” module was used to draw the Venn diagram of the two targets, and the common target—that is, the direct target of hepatotoxicity induced by MA in rats—was obtained by finding their intersection.

5.4.4. Construction and Analysis of Protein–protein Interaction (PPI) Network

The potential hepatotoxic targets of MA were imported into the String database (<https://stringdb.org/>, accessed on 14 April 2022) to obtain the interaction data between genes, and the results were imported into Cytoscape 3.7.2 software for PPI network visualization. The topological analysis of PPI network was carried out by using the function “Network Analyzer”. The size and color of nodes in the interactive network were related to the “Degree” of this node, that is, the larger the “Degree” value of this node, the bigger the node and the redder its color. The width of an edge showed strength of interaction between the two nodes connected by this edge; that is, the stronger the interaction, the wider the edge.

5.4.5. Gene Ontology (GO) Analysis and Kyoto Encyclopedia of Genes and Genomes (KEGG) Pathway Enrichment Analysis

GO and KEGG analysis of target genes in PPI network was carried out using the String database, and the files “enrichment.component”, “enrichment.Function”, “enrichment.Process” and “enrichment.KEGG” were obtained. GraphPad-Prism 6.0 and Omicshare (<http://www.omicshare.com/tools/index.php/>, accessed on 14 April 2022) were used to visualize these four files.

5.5. Western Blot Analysis

Proteins extracted from liver tissues of each group were used in Western blotting to validate the network toxicology results. The liver tissues were lysed using lysis buffer containing a protease inhibitor cocktail to extract total liver protein of rats in each group. The protein concentrations of samples were determined using the BCA method, and proteins were denatured via boiling for 5 min. Next, 40 µg of total protein in each group was loaded and separated using sodium dodecyl sulfate–polyacrylamide (SDS) and transferred to methanol-activated polyvinylidene fluoride membranes (Millipore). Next, the membrane was blocked in TBST containing 5% skimmed milk for 1 h at room temperature, and incubated with primary antibody (HMOX1, 1:2000, Boster; IL2, 1:2000, Bioss; Caspase-3, 1:1000, Servicebio; GAPDH, 1:6000, Abcam) overnight, followed by incubation with the secondary antibodies (HRP-Goat anti rabbit, HRP-Goat anti mouse, 1:50,000, Searcare) at room temperature for another 30 min. ECL was used for protein imaging and development.

Supplementary Materials: The following supporting information can be downloaded at: <https://www.mdpi.com/article/10.3390/toxins14070486/s1>. Table S1: Trends of differential metabolites involved in metabolic pathways; Table S2: Results of hepatotoxicity targets on online database; Table S3: Potential direct targets of hepatotoxicity induced by MA. Figure S1: The summarized metabolic pathways in the low dose and high dose rats.

Author Contributions: Conceptualization, Q.C. and K.Z.; methodology, Q.C. and K.Z.; investigation, M.J., J.J., D.C. and Y.Y.; writing—original draft, Q.C. and K.Z.; writing—review and editing, J.Z. and F.L.; funding acquisition, F.L. All authors have read and agreed to the published version of the manuscript.

Funding: This research was funded by the National Natural Science Foundation of China, grant number 81973479.

Institutional Review Board Statement: The animal study protocol was approved by the Animal Ethics Committee of Beijing University of Chinese Medicine (Approval No.: BUCM-4-2021071901-3023, Approval date: 19 July 2021).

Informed Consent Statement: Not applicable.

Data Availability Statement: The data presented in this study are available in this article and Supplementary Materials.

Conflicts of Interest: The authors declare no conflict of interest.

References

1. Tan, P.; Chen, X.; He, R.; Liu, Y. Analysis of the metabolites of mesaconitine in rat blood using ultrafast liquid chromatography and electrospray ionization mass spectrometry. *Pharmacogn. Mag.* **2014**, *10*, 101–105.
2. Sun, Z.; Yang, L.; Zhao, L.; Cui, R.; Yang, W. Neuropharmacological Effects of Mesaconitine: Evidence from Molecular and Cellular Basis of Neural Circuit. *Neural Plast.* **2020**, *2020*, 8814531.
3. Zhao, L.; Sun, Z.; Yang, L.; Cui, R.; Yang, W.; Li, B. Neuropharmacological effects of Aconiti Lateralis Radix Praeparata. *Clin. Exp. Pharmacol. Physiol.* **2020**, *47*, 531–542.
4. Hikino, H.; Murayama, M. Mechanism of the antinociceptive action of mesaconitine: Participation of brain stem and lumbar enlargement. *Br. J. Pharmacol.* **1985**, *85*, 575–580.
5. Li, X.; Ou, X.; Luo, G.; Ou, X.; Xie, Y.; Ying, M.; Qu, W.; Zuo, H.; Qi, X.; Wang, Y.; et al. Mdr1a, Bcrp and Mrp2 regulate the efficacy and toxicity of mesaconitine and hyphaconitine by altering their tissue accumulation and in vivo residence. *Toxicol. Appl. Pharmacol.* **2020**, *409*, 115332.
6. Ye, L.; Tang, L.; Gong, Y.; Lv, C.; Zheng, Z.; Jiang, Z.; Liu, Z. Characterization of metabolites and human P450 isoforms involved in the microsomal metabolism of mesaconitine. *Xenobiotica* **2011**, *41*, 46–58.
7. Mitamura, M.; Horie, S.; Sakaguchi, M.; Someya, A.; Tsuchiya, S.; Van de Voorde, J.; Murayama, T.; Watanabe, K. Mesaconitine-induced relaxation in rat aorta: Involvement of Ca²⁺ influx and nitric-oxide synthase in the endothelium. *Eur. J. Pharmacol.* **2002**, *436*, 217–225.
8. Nesterova, Y.V.; Povetieva, T.N.; Suslov, N.I.; Semenov, A.A.; Pushkarskiy, S.V. Antidepressant activity of diterpene alkaloids of *Aconitum baicalense* Turcz. *Bull. Exp. Biol. Med.* **2011**, *151*, 425–428.
9. Wang, X.C.; Jia, Q.Z.; Yu, Y.L.; Wang, H.D.; Guo, H.C.; Ma, X.D.; Liu, C.T.; Chen, X.Y.; Miao, Q.F.; Guan, B.C.; et al. Inhibition of the INa/K and the activation of peak INa contribute to the arrhythmogenic effects of aconitine and mesaconitine in guinea pigs. *Acta Pharmacol. Sin.* **2021**, *42*, 218–229.
10. Hsu, S.S.; Liang, W.Z. Cytotoxic Effects of Mesaconitine, the *Aconitum carmichaelii* Debx Bioactive Compound, on HBEC-5i Human Brain Microvascular Endothelial Cells: Role of Ca²⁺ Signaling-Mediated Pathway. *Neurotox. Res.* **2021**, *39*, 256–265.
11. Ogura, J.; Mitamura, M.; Someya, A.; Shimamura, K.; Takayama, H.; Aimi, N.; Horie, S.; Murayama, T. Mesaconitine-induced relaxation in rat aorta: Role of Na⁺/Ca²⁺ exchangers in endothelial cells. *Eur. J. Pharmacol.* **2004**, *483*, 139–146.
12. Zhou, W.; Liu, H.; Qiu, L.Z.; Yue, L.X.; Zhang, G.J.; Deng, H.F.; Ni, Y.H.; Gao, Y. Cardiac efficacy and toxicity of aconitine: A new frontier for the ancient poison. *Med. Res. Rev.* **2021**, *41*, 1798–1811.
13. Qin, Y.; Wang, J.B.; Zhao, Y.L.; Shan, L.M.; Li, B.C.; Fang, F.; Jin, C.; Xiao, X.H. Establishment of a bioassay for the toxicity evaluation and quality control of Aconitum herbs. *J. Hazard. Mater.* **2012**, *199–200*, 350–357.
14. Cai, Y.; Gao, Y.; Tan, G.; Wu, S.; Dong, X.; Lou, Z.; Zhu, Z.; Chai, Y. Myocardial lipidomics profiling delineate the toxicity of traditional Chinese medicine Aconiti Lateralis radix praeparata. *J. Ethnopharmacol.* **2013**, *147*, 349–356.
15. Chung, J.Y.; Lee, S.J.; Lee, H.J.; Bong, J.B.; Lee, C.H.; Shin, B.S.; Kang, H.G. Aconitine Neurotoxicity According to Administration Methods. *J. Clin. Med.* **2021**, *10*, 2149.
16. Xiao, F.; Qiu, J.; Zhao, Y. Exploring the Potential Toxicological Mechanisms of Vine Tea on the Liver Based on Network Toxicology and Transcriptomics. *Front. Pharmacol.* **2022**, *13*, 855926.
17. Lu, X.; Huang, H.; Fu, X.; Chen, C.; Liu, H.; Wang, H.; Wu, D. The Role of Endoplasmic Reticulum Stress and NLRP3 Inflammasome in Liver Disorders. *Int. J. Mol. Sci.* **2022**, *23*, 3528.
18. Fusco, R.; Gugliandolo, E.; Siracusa, R.; Scuto, M.; Cordaro, M.; D’Amico, R.; Evangelista, M.; Peli, A.; Peritore, A.F.; Impellizzeri, D.; et al. Formyl Peptide Receptor 1 Signaling in Acute Inflammation and Neural Differentiation Induced by Traumatic Brain Injury. *Biology* **2020**, *9*, 238.
19. Mihajlovic, M.; Vinken, M. Mitochondria as the Target of Hepatotoxicity and Drug-Induced Liver Injury: Molecular Mechanisms and Detection Methods. *Int. J. Mol. Sci.* **2022**, *23*, 3315.
20. Yang, M.; Ji, X.; Zuo, Z. Relationships between the Toxicities of Radix Aconiti Lateralis Preparata (Fuzi) and the Toxicokinetics of Its Main Diester-Diterpenoid Alkaloids. *Toxins* **2018**, *10*, 391.
21. Zhou, H.; Zhang, P.; Hou, Z.; Xie, J.; Wang, Y.; Yang, B.; Xu, Y.; Li, Y. Research on the Relationships between Endogenous Biomarkers and Exogenous Toxic Substances of Acute Toxicity in Radix Aconiti. *Molecules* **2016**, *21*, 1623.

22. Tan, Y.; Ko, J.; Liu, X.; Lu, C.; Li, J.; Xiao, C.; Li, L.; Niu, X.; Jiang, M.; He, X.; et al. Serum metabolomics reveals betaine and phosphatidylcholine as potential biomarkers for the toxic responses of processed *Aconitum carmichaelii* Debx. *Mol. Biosyst.* **2014**, *10*, 2305–2316.
23. Ji, X.; Yang, M.; Or, K.H.; Yim, W.S.; Zuo, Z. Tissue Accumulations of Toxic Aconitum Alkaloids after Short-Term and Long-Term Oral Administrations of Clinically Used *Radix Aconiti Lateralis* Preparations in Rats. *Toxins* **2019**, *11*, 353.
24. Zhang, K.; Liu, C.; Yang, T.; Li, X.; Wei, L.; Chen, D.; Zhou, J.; Yin, Y.; Yu, X.; Li, F. Systematically explore the potential hepatotoxic material basis and molecular mechanism of *Radix Aconiti Lateralis* based on the concept of toxicological evidence chain (TEC). *Ecotoxicol. Environ. Saf.* **2020**, *205*, 111342.
25. Sun, B.; Wu, S.; Li, L.; Li, H.; Zhang, Q.; Chen, H.; Li, F.; Dong, F.; Yan, X. A metabolomic analysis of the toxicity of *Aconitum* sp. alkaloids in rats using gas chromatography/mass spectrometry. *Rapid Commun. Mass Spectrom.* **2009**, *23*, 1221–1228.
26. Bi, C.; Zhang, T.; Li, Y.; Zhao, H.; Zhang, P.; Wang, Y.; Xu, Y.; Gu, K.; Liu, Y.; Yu, J.; et al. A Proteomics- and Metabolomics-Based Study Revealed That Disorder of Palmitic Acid Metabolism by Aconitine Induces Cardiac Injury. *Chem. Res. Toxicol.* **2020**, *33*, 3031–3040.
27. Fujita, Y.; Terui, K.; Fujita, M.; Kakizaki, A.; Sato, N.; Oikawa, K.; Aoki, H.; Takahashi, K.; Endo, S. Five cases of aconite poisoning: Toxicokinetics of aconitines. *J. Anal. Toxicol.* **2007**, *31*, 132–137.
28. Yan, L.; Wang, P.; Zhao, C.; Fan, S.; Lin, H.; Guo, Y.; Ma, Z.; Qiu, L. Toxic responses of liver in *Lateolabrax maculatus* during hypoxia and re-oxygenation. *Aquat. Toxicol.* **2021**, *236*, 105841.
29. He, T.; Liu, C.; Li, M.; Wang, M.; Liu, N.; Zhang, D.; Han, S.; Li, W.; Chen, S.; Yuan, R.; et al. Integrating non-targeted metabolomics and toxicology networks to study the mechanism of Esculentoside A-induced hepatotoxicity in rats. *J. Biochem. Mol. Toxicol.* **2021**, *35*, 1–15.
30. Hu, Q.; Wei, S.; Wen, J.; Zhang, W.; Jiang, Y.; Qu, C.; Xiang, J.; Zhao, Y.; Peng, X.; Ma, X. Network pharmacology reveals the multiple mechanisms of Xiaochaihu decoction in the treatment of non-alcoholic fatty liver disease. *BioData Min.* **2020**, *13*, 11.
31. Yang, Z.; Mo, Y.; Cheng, F.; Zhang, H.; Shang, R.; Wang, X.; Liang, J.; Liu, Y.; Hao, B. Antioxidant Effects and Potential Molecular Mechanism of Action of *Limonium aureum* Extract Based on Systematic Network Pharmacology. *Front. Vet. Sci.* **2022**, *8*, 775490.
32. Nishiyama, Y.; Goda, N.; Kanai, M.; Niwa, D.; Osanai, K.; Yamamoto, Y.; Senoo-Matsuda, N.; Johnson, R.S.; Miura, S.; Kabe, Y.; et al. HIF-1 α induction suppresses excessive lipid accumulation in alcoholic fatty liver in mice. *J. Hepatol.* **2012**, *56*, 441–447.
33. Liang, X.; Zhang, L.; Natarajan, S.K.; Becker, D.F. Proline mechanisms of stress survival. *Antioxid. Redox Signal.* **2013**, *19*, 998–1011.
34. Leal, J.; Teixeira-Santos, L.; Pinho, D.; Afonso, J.; Carvalho, J.; Bastos, M.d.L.; Albino-Teixeira, A.; Fraga, S.; Sousa, T. l-proline supplementation improves nitric oxide bioavailability and counteracts the blood pressure rise induced by angiotensin II in rats. *Nitric Oxide Biol. Chem.* **2019**, *82*, 1–11.
35. Su, X.; Yu, W.; Liu, A.; Wang, C.; Li, X.; Gao, J.; Liu, X.; Jiang, W.; Yang, Y.; Lv, S. San-Huang-Yi-Shen Capsule Ameliorates Diabetic Nephropathy in Rats Through Modulating the Gut Microbiota and Overall Metabolism. *Front. Pharmacol.* **2022**, *12*, 808867.
36. Liu, R.; Yan, X. Oxidative stress in corneal stromal cells contributes to the development of keratoconus in a rabbit model. *Eur. J. Ophthalmol.* **2021**, *31*, 3518–3524.
37. Liu, Y.; Chen, X.; Liu, Y.; Chen, T.; Zhang, Q.; Zhang, H.; Zhu, Z.; Chai, Y.; Zhang, J. Metabolomic study of the protective effect of Gandi capsule for diabetic nephropathy. *Chem. Biol. Interact.* **2019**, *314*, 108815.
38. Anesi, A.; Rubert, J.; Oluwagbemigun, K.; Orozco-Ruiz, X.; Nöthlings, U.; Breteler, M.; Mattivi, F. Metabolic Profiling of Human Plasma and Urine, Targeting Tryptophan, Tyrosine and Branched Chain Amino Acid Pathways. *Metabolites* **2019**, *9*, 261.
39. Tu, C.; Niu, M.; Li, C.; Liu, Z.; He, Q.; Li, R.; Zhang, Y.; Xiao, X.; Wang, J. Network pharmacology oriented study reveals inflammatory state-dependent dietary supplement hepatotoxicity responses in normal and diseased rats. *Food Funct.* **2019**, *10*, 3477–3490.
40. Kumar, N.; Surani, S.; Udeani, G.; Mathew, S.; John, S.; Sajan, S.; Mishra, J. Drug-induced liver injury and prospect of cytokine based therapy; A focus on IL-2 based therapies. *Life Sci.* **2021**, *278*, 119544.
41. Nakagawa, K.; Miller, F.N.; Sims, D.E.; Lentsch, A.B.; Miyazaki, M.; Edwards, M.J. Mechanisms of interleukin-2-induced hepatic toxicity. *Cancer Res.* **1996**, *56*, 507–510.
42. Strieter, R.M.; Remick, D.G.; Lynch, J.P.; Spengler, R.N.; Kunkel, S.L. Interleukin-2-induced tumor necrosis factor- α (TNF- α) gene expression in human alveolar macrophages and blood monocytes. *Am. Rev. Respir. Dis.* **1989**, *139*, 335–342.
43. Abu-Amara, M.; Yang, S.Y.; Tapuria, N.; Fuller, B.; Davidson, B.; Seifalian, A. Liver ischemia/reperfusion injury: Processes in inflammatory networks—A review. *Liver Transplant.* **2010**, *16*, 1016–1032.
44. Shuh, M.; Bohorquez, H.; Loss, G.E.; Cohen, A.J. Tumor Necrosis Factor- α : Life and Death of Hepatocytes During Liver Ischemia/Reperfusion Injury. *Ochsner J.* **2013**, *13*, 119–130.
45. Guha, M.; Mackman, N. The phosphatidylinositol 3-kinase-Akt pathway limits lipopolysaccharide activation of signaling pathways and expression of inflammatory mediators in human monocytic cells. *J. Biol. Chem.* **2002**, *277*, 32124–32132.
46. Díaz-Guerra, M.J.; Castrillo, A.; Martín-Sanz, P.; Bosca, L. Negative regulation by phosphatidylinositol 3-kinase of inducible nitric oxide synthase expression in macrophages. *J. Immunol.* **1999**, *162*, 6184–6190.
47. Li, X.; Wu, Y.; Zhang, W.; Gong, J.; Cheng, Y. Pre-conditioning with tanshinone IIA attenuates the ischemia/reperfusion injury caused by liver grafts via regulation of HMGB1 in rat Kupffer cells. *Biomed. Pharmacother.* **2017**, *89*, 1392–1400.
48. Xiao, Q.; Ye, Q.; Wang, W.; Xiao, J.; Fu, B.; Xia, Z.; Zhang, X.; Liu, Z.; Zeng, X. Mild hypothermia pretreatment protects against liver ischemia reperfusion injury via the PI3K/AKT/FOXO3a pathway. *Mol. Med. Rep.* **2017**, *16*, 7520–7526.

49. Shen, Y.; Shen, X.; Cheng, Y.; Liu, Y. Myricitrin pretreatment ameliorates mouse liver ischemia reperfusion injury. *Int. Immunopharmacol.* **2020**, *89*, 107005.
50. Reyes-Gordillo, K.; Shah, R.; Arellanes-Robledo, J.; Cheng, Y.; Ibrahim, J.; Tuma, P.L. Akt1 and Akt2 Isoforms Play Distinct Roles in Regulating the Development of Inflammation and Fibrosis Associated with Alcoholic Liver Disease. *Cells* **2019**, *8*, 1337.
51. O'Neil, J.D.; Ammit, A.J.; Clark, A.R. MAPK p38 regulates inflammatory gene expression via tristetraprolin: Doing good by stealth. *Int. J. Biochem. Cell Biol.* **2018**, *94*, 6–9.
52. Fusco, R.; Cordaro, M.; Siracusa, R.; D'Amico, R.; Genovese, T.; Gugliandolo, E.; Peritore, A.F.; Crupi, R.; Impellizzeri, D.; Cuzzocrea, S.; et al. Biochemical Evaluation of the Antioxidant Effects of Hydroxytyrosol on Pancreatitis-Associated Gut Injury. *Antioxidants* **2020**, *9*, 781.
53. Yu, Y.B.; Zhuang, H.Z.; Ji, X.J.; Dong, L.; Duan, M.L. Hydroxytyrosol suppresses LPS-induced intrahepatic inflammatory responses via inhibition of ERK signaling pathway activation in acute liver injury. *Eur. Rev. Med. Pharmacol. Sci.* **2020**, *24*, 6455–6462.
54. Beggs, K.M.; Maiuri, A.R.; Fullerton, A.M.; Poulsen, K.L.; Breier, A.B.; Ganey, P.E.; Roth, R.A. Trovafloxacin-induced replication stress sensitizes HepG2 cells to tumor necrosis factor- α -induced cytotoxicity mediated by extracellular signal-regulated kinase and ataxia telangiectasia and Rad3-related. *Toxicology* **2015**, *331*, 35–46.
55. Chen, S.; Zhang, Z.; Wu, Y.; Shi, Q.; Yan, H.; Mei, N.; Tolleson, W.H.; Guo, L. Endoplasmic Reticulum Stress and Store-Operated Calcium Entry Contribute to Uronic Acid-Induced Toxicity in Hepatic Cells. *Toxicol. Sci.* **2015**, *146*, 116–126.
56. Hu, J.; Ramshesh, V.K.; McGill, M.R.; Jaeschke, H.; Lemasters, J.J. Low Dose Acetaminophen Induces Reversible Mitochondrial Dysfunction Associated with Transient c-Jun N-Terminal Kinase Activation in Mouse Liver. *Toxicol. Sci.* **2016**, *150*, 204–215.
57. Poulsen, K.L.; Albee, R.P.; Ganey, P.E.; Roth, R.A. Trovafloxacin potentiation of lipopolysaccharide-induced tumor necrosis factor release from RAW 264.7 cells requires extracellular signal-regulated kinase and c-Jun N-Terminal Kinase. *J. Pharmacol. Exp. Ther.* **2014**, *349*, 185–191.
58. Wu, Y.; Beland, F.A.; Chen, S.; Liu, F.; Guo, L.; Fang, J.L. Mechanisms of tolvaftan-induced toxicity in HepG2 cells. *Biochem. Pharmacol.* **2015**, *95*, 324–336.
59. Cheng, C.W.; Liu, M.H.; Tang, H.Y.; Cheng, M.L.; Wang, C.H. Factors associated with elevated plasma phenylalanine in patients with heart failure. *Amino Acids* **2021**, *53*, 149–157.
60. Chen, W.S.; Wang, C.H.; Cheng, C.W.; Liu, M.H.; Chu, C.M.; Wu, H.P.; Huang, P.C.; Lin, Y.T.; Ko, T.; Chen, W.H.; et al. Elevated plasma phenylalanine predicts mortality in critical patients with heart failure. *ESC Heart Fail.* **2020**, *7*, 2884–2893.
61. Wang, M.; Zhang, J.; Gong, N. Role of the PI3K/Akt signaling pathway in liver ischemia reperfusion injury: A narrative review. *Ann. Palliat. Med.* **2022**, *11*, 806–817.
62. Wu, D.; Yang, C.; Yang, M.; Wu, Y.; Mao, Y.; Zhou, X.; Wang, J.; Yuan, Z.; Wu, J. Citrinin-Induced Hepatotoxicity in Mice Is Regulated by the Ca²⁺/Endoplasmic Reticulum Stress Signaling Pathway. *Toxins* **2022**, *14*, 259.
63. Rehman, M.U.; Tahir, M.; Khan, A.Q.; Khan, R.; Lateef, A.; Hamiza, O.O.; Ali, F.; Sultana, S. Diosmin protects against trichloroethylene-induced renal injury in Wistar rats: Plausible role of p53, Bax and caspases. *Br. J. Nutr.* **2013**, *110*, 699–710.
64. Prokhorova, E.A.; Kopeina, G.S.; Lavrik, I.N.; Zhivotovsky, B. Apoptosis regulation by subcellular relocation of caspases. *Sci. Rep.* **2018**, *8*, 12199.
65. Wang, Z.; Hao, W.; Hu, J.; Mi, X.; Han, Y.; Ren, S.; Jiang, S.; Wang, Y.; Li, X.; Li, W. Maltol Improves APAP-Induced Hepatotoxicity by Inhibiting Oxidative Stress and Inflammation Response via NF- κ B and PI3K/Akt Signal Pathways. *Antioxidants* **2019**, *8*, 395.
66. Cui, M.; Huang, Y.; Zhao, Y.; Zheng, J. New insights for FOXO and cell-fate decision in HIV infection and HIV associated neurocognitive disorder. *Adv. Exp. Med. Biol.* **2009**, *665*, 143–159.
67. Lau, C.J.; Koty, Z.; Nalbantoglu, J. Differential response of glioma cells to FOXO1-directed therapy. *Cancer Res.* **2009**, *69*, 5433–5440.
68. Su, Y.W.; Hao, Z.; Hirao, A.; Yamamoto, K.; Lin, W.J.; Young, A.; Duncan, G.S.; Yoshida, H.; Wakeham, A.; Lang, P.A.; et al. 14-3-3 σ regulates B-cell homeostasis through stabilization of FOXO1. *Proc. Natl. Acad. Sci. USA* **2011**, *108*, 1555–1560.
69. Sullivan, J.A.; Kim, E.H.; Plisch, E.H.; Suresh, M. FOXO3 regulates the CD8 T cell response to a chronic viral infection. *J. Virol.* **2012**, *86*, 9025–9034.
70. Tan, M.; Cheng, Y.; Zhong, X.; Yang, D.; Jiang, S.; Ye, Y.; Ding, M.; Guan, G.; Yang, D.; Zhao, X. LNK promotes granulosa cell apoptosis in PCOS via negatively regulating insulin-stimulated AKT-FOXO3 pathway. *Aging* **2021**, *13*, 4617–4633.
71. Sun, F.; Zhou, J.L.; Wei, S.X.; Jiang, Z.W.; Peng, H. Glucocorticoids induce osteonecrosis of the femoral head in rats via PI3K/AKT/FOXO1 signaling pathway. *PeerJ* **2022**, *10*, e13319.
72. Burgering, B.M.; Kops, G.J. Cell cycle and death control: Long live Forkheads. *Trends Biochem. Sci.* **2002**, *27*, 352–360.